



On the quality and structural characteristics of oligo(ethylene glycol) assemblies on gold: An experimental and theoretical study

Ramūnas Valiokas^{a,d,*}, Lyuba Malysheva^b, Alexander Onipko^{b,d}, Hung-Hsun Lee^d, Živilė Ruželė^a, Sofia Svedhem^d, Stefan C.T. Svensson^d, Ulrik Gelius^c, Bo Liedberg^{d,**}

^a Department of Functional Nanomaterials, Institute of Physics, Savanorių 231, LT-02300 Vilnius, Lithuania

^b Bogolyubov Institute for Theoretical Physics, Kiev 03143, Ukraine

^c Department of Physics, Uppsala University, S-75121 Uppsala, Sweden

^d Division of Molecular Physics, Department of Physics and Measurement Technology, Linköping University, S-581 83 Linköping, Sweden

ARTICLE INFO

Article history:

Available online 1 April 2009

Keywords:

Self-assembled monolayers
Oligo(ethylene glycol)
Hydrogen bonding
Infrared spectroscopy
X-ray photoelectron spectroscopy
Ab initio modeling

ABSTRACT

This paper presents results of several years of experimental and theoretical work on a library of oligo(ethylene glycol)-containing self-assembled monolayers (OEG SAMs) on gold. The library consists of 15 different thiol compounds, which all contain alkyl and OEG portions of different length, as well as amide moieties forming a stabilizing lateral hydrogen bonding network. We have investigated the quality, conformation, orientation, defect structure and infrared (IR) signatures of these OEG SAMs prepared by spontaneous adsorption from dilute solutions. It is shown that solution concentration and incubation time are important factors to obtain high quality SAMs, in particular for those containing long OEG chains. Further on, the thiol compounds should contain a sufficiently long alkyl spacer to provide in plane van der Waals interactions strong enough to govern the formation of a densely packed alkylthiolate overlayer on the Au(111) surface. Such a highly ordered alkyl support, which is additionally stabilized by the lateral hydrogen bonds, enables us to vary the length of the terminal OEG portion from 1 to at least 12, without affecting the integrity and conformational characteristics of the supporting (alkyl) part of the SAM. Also, we discuss the importance of appropriate modeling tools to advance the understanding of IR signatures of the OEG SAMs. Finally, we demonstrate the generality of our “modular approach” by analyzing the structure of OEG SAMs formed by compounds extended with an additional terminal amide and an alkyl tail. Thus, the SAMs discussed herein provide an attractive platform for construction of advanced nanoarchitectures on surfaces, not only limited to biomaterials and fouling applications.

© 2009 Elsevier B.V. All rights reserved.

1. Introduction

Self-assembled monolayers (SAMs) on gold formed by alkylthiol derivatives with a terminal moiety consisting of oligo(ethylene glycol) (OEG) have become an attractive strategy in designing biointerfaces. These bifunctional materials were introduced by Whitesides and co-workers in an attempt to create 2D architectures with favorable protein resistance properties [1]. Since then, substantial efforts have been undertaken to advance the understanding about the relatively weak interactions between the OEG-terminated SAMs and complex biological fluids [2–4]. For example, Grunze and co-workers proposed a model, which is based on the hydrogen bond formation between water molecules and

a conformationally disordered OEG terminus [5]. However, the water–OEG interactions remain to be the subject of extensive investigations [6,7]. Based on the obtained knowledge, the technological applications are diverse and the OEG SAMs constitute today a reliable platform for biosensor, protein and cell array fabrication. Moreover, well-defined molecular interfaces have been built for assembly of biomimetic cell membranes, which can be supported on a hydrogel-like OEG layer [8,9].

We have previously reported on the structural aspects of the OEG assemblies on gold [10–18]. Besides explaining the role of the OEG conformation and chain length on its interactions with complex protein systems [19], we have systematically studied the importance of synthetically introduced functional entities to explore the importance of intermolecular interactions on the stability of OEG SAM-based biointerfaces. Our experimental and theoretical studies have led to the conclusion that relatively short OEG motifs offer an attractive strategy to design surface-supported molecular architectures with novel and unique properties, not only limited to biomaterials applications. We believe that OEG-containing or OEG-

* Corresponding author at: Department of Functional Nanomaterials, Institute of Physics, Savanorių 231, LT-02300 Vilnius, Lithuania.

** Corresponding author.

E-mail addresses: valiokas@ar.fi.lt (R. Valiokas), bolie@ifm.liu.se (B. Liedberg).

Table 1
Full library of thiol compounds used to study the quality and structural characteristics of oligo(ethylene glycol)-containing self-assembled monolayers on gold.

Chemical structure	Shortened name
$\text{HS}(\text{CH}_2)_m\text{-CONH}-(\text{CH}_2\text{CH}_2\text{O})_n\text{-H}$, $m = 2, 5, 11$; $n = 4, 6$	C_mEG_n
$\text{HS}(\text{CH}_2)_{15}\text{-CONH}-(\text{CH}_2\text{CH}_2\text{O})_n\text{-H}$, $n = 1, 2, 4, 6, 8, 10, 12$	C_{15}EG_n
$\text{HS}(\text{CH}_2)_{15}\text{-CONH}-(\text{CH}_2\text{CH}_2\text{O})_6\text{CH}_2\text{-CONH-CH}_3$	$\text{C}_{15}\text{EG}_6\text{C}_1$
$\text{HS}(\text{CH}_2)_{15}\text{-CONH}-(\text{CH}_2\text{CH}_2\text{O})_6\text{CH}_2\text{-CONH}-(\text{CH}_2)_{15}\text{-CH}_3$	$\text{C}_{15}\text{EG}_6\text{C}_{16}$

based SAMs can be considered as a generic platform in nanoscience and nanotechnology. Owing to their well-defined and precisely controlled conformational and phase characteristics [12,20,21], the OEGs can significantly extend the possibilities to generate assemblies with a much higher degree of complexity as compared to the conventional, relatively structurally simple alkylthiolate SAMs. For example, recently, we have reported on the formation of highly ordered SAMs with an improved thermal stability [22]. In this particular case the SAM was 60 Å thick, a thickness, which might be crucial for controlling substrate “quenched” effects in advanced nanoplasmonic devices [23,24] and other nanoscopic architectures.

The investigation of self-assembly of structurally complex, strongly interacting compounds is not trivial. More systematic studies are needed in order to be able to develop reliable protocols for assembly of advanced nanoarchitectures on solid surfaces [25]. Therefore, in the present work we have combined experimental and theoretical efforts to shed light on the quality, molecular orientation and defect structure of OEG-containing SAMs. We have used a powerful set of surface spectroscopy techniques, namely X-ray photoelectron spectroscopy (XPS) and infrared reflection–absorption spectroscopy (IRAS) together with contact angle goniometry and null ellipsometry, to reveal the influence of OEG SAM preparation conditions, as well as the importance of a proper combination of oligomer chain length and specific intermolecular interactions, introduced via an amide linking group (Table 1). Also, based on the knowledge obtained from an extensive ab initio modeling [14–18,26], we discuss in detail assignments and defects signatures observed in IR spectra of OEG SAMs and the most likely orientation of the molecular constituents as a function of complexity.

2. Materials and methods

2.1. Sample preparation

Gold films 2000 Å thick were prepared on silicon (100) substrates primed with a 25 Å titanium layer using an electron beam evaporation system (Balzers UMS 500 P). The base pressure was 10^{-9} mbar. The evaporation pressure was kept on the low 10^{-7} mbar scale, and the evaporation rate was 10 Å s^{-1} .

Gold substrates were first cleaned in a 5:1:1 mixture of water, 30% hydrogen peroxide and 25% ammonia at 80 °C for 5 min, rinsed in deionized (MilliQ) water and incubated with ethanolic solutions of 1 mM and 20 μM concentrations of OEG-containing thiol compounds. The synthesis of the compounds is described elsewhere by Svedhem et al. [27] and Lee et al. [28]. The alcohol thiol ($\text{HS}(\text{CH}_2)_{16}\text{-OH}$) was a generous gift from GE Healthcare Bio-Sciences AB. The adsorption time varied from 10 min, 24 h to 19 days. After incubation with the thiol solutions the samples were rinsed and ultrasonicated in ethanol and blown dry in argon or nitrogen gas immediately before the XPS or IRAS analyses.

2.2. XPS

The XPS experiments were carried out on SCIENTA ESCA 300 spectrometer. Monochromatized Al K_{α} radiation (1486.6 eV) was used, and the photoelectron take-off angles were 90° and 10° rela-

tive to the surface. The power of the X-ray gun was 8 or 6 kW. A pass energy of 300 eV, and a width of the analyzer entrance slit of 0.8 mm gave 0.5 eV resolution of the spectrometer [29]. The pressure in the measurement chamber was held on the low 10^{-9} mbar scale. The temperature was around 303 K. Several spots on each sample were investigated, and the spots were selected so that the possibility of X-ray induced damage of the sample was minimized. The spectra recorded at a take-off angle (TOA) of 90° are shown as sums of four measurements on four different spots on the sample, and those at TOA = 10° as sums of three measurements on three different spots. It should be mentioned that the OEG compounds showed a certain drift in peak position of the C1s and O1s regions towards higher binding energies (most likely due to charging) during collection of spectra from several spots on the sample. In the shown spectra are the core level peaks fixed at the position of the last measurement by adding a correction factor (<0.09 eV) to the preceding spectra.

2.3. Infrared spectroscopy

The reflection–absorption (RA) spectra were recorded on a Bruker IFS 66 system, equipped with a grazing angle (85°) infrared reflection accessory and a liquid nitrogen cooled-MCT detector. The measurement chamber was continuously purged with nitrogen gas during the measurements. The acquisition time was around 10 min. The RA spectra were recorded at 2 cm^{-1} resolution and a three-term Blackmann–Harris apodization function was applied to the interferograms before Fourier transformation. A spectrum of a deuterated hexadecanethiol ($\text{HS}(\text{CD}_2)_{15}\text{CD}_3$) SAM on a gold was recorded and used as a reference.

2.4. Ab initio modeling

Wide-scale ab initio calculations of structural and spectral properties of the SAM constituents were used to understand the experimental data. Considering the molecular weight and structural complexity of the compounds under investigation, the first-principle results could be obtained only for isolated molecules. The model infrared RA spectra were obtained as the sum of Lorentzian-shaped peaks, each centered at the fundamental mode frequency. The molecular optimized geometries, vibrational frequencies, and transition dipole moments were calculated by the DFT methods, as provided by the Gaussian-03 suite of programs. Most of our calculations exploited the BP86 exchange–correlation functional (a GGA functional combining the Becke 88 exchange and Perdew 86 correlation functional) with 6-31G* basis set.

3. Results and discussion

3.1. Tuning the preparation conditions of SAMs with complex OEG tails

At the initial stage, we developed a series of OEG-terminated and amide-containing alkylthiols on gold, $\text{C}_{15}\text{EG}_{1,2,4,6}$, and studied these assemblies by a set of surface analysis techniques, including IRAS and temperature-programmed desorption [10,12,13]. We demonstrated that a proper combination of oligomer chain length and specific intermolecular interactions, introduced via the linking group, lead to new and interesting phase properties of the OEG SAMs. For example, the compounds with terminal EG_2 and EG_4 portions form SAMs with a dominating all trans OEG phase, whereas EG_6 -terminated SAMs displayed distinctive OEG-related peaks in the RA spectrum, which indicate the formation of a helical OEG portion [10]. Upon heating the samples in ultrahigh vacuum we observed a relatively sharp and fully reversible transition of the EG_6 portion from helical at room temperature to all trans at temperatures above $\sim 60 \text{ °C}$ [11]. Also, we observed subtle

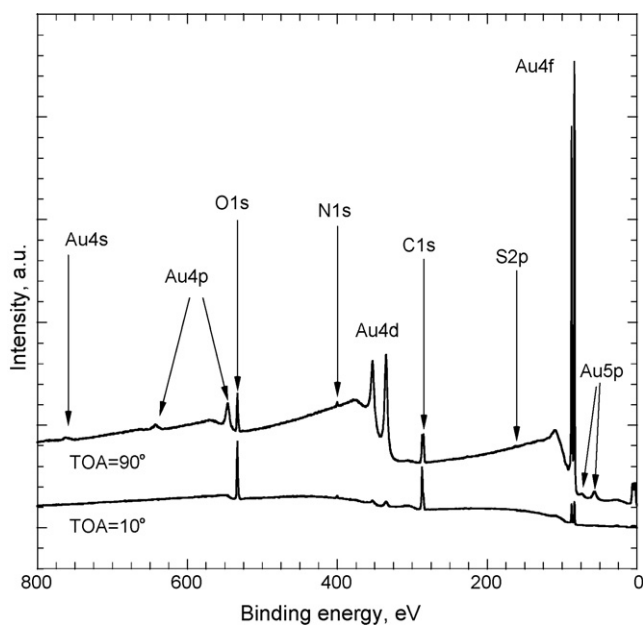


Fig. 1. XPS survey spectra of $C_{15}EG_6$ SAM on gold obtained at two take-off angles, 90° and 10° .

preparation-dependent structural differences of $C_{15}EG_4$ and $C_{15}EG_6$ SAMs, which were visible as slight shifts and/or intensity changes of the all trans and helical OEG peaks in the infrared spectra. Therefore, here we report structural details of $C_{15}EG_{1,2,4,6}$ SAMs obtained using primarily XPS. Although the core electrons are rather insensitive to the conformational properties of the OEGs, they do provide important information about I) the chemical composition of the SAM, II) the interaction(s) between the thiol group and the gold surface including the state of oxidation of the thiol, and III) the orientation of the constituent molecules in the SAM.

X-ray photoelectron survey spectra are recorded at 90° and 10° take-off angles (TOA) for all four compounds, and Fig. 1 shows the survey spectra of the $C_{15}EG_6$ SAM. The characteristic Au4f peaks dominate the 90° spectra, but peaks due to core level electrons of the SAM can be observed as well. The O1s and C1s peaks appearing at 533.5 and in the range 285–287 eV, respectively, are easily identified. A weak feature around 400.4 eV originating from N1s photoelectrons of the amide group is also seen. The S2p electrons, that typically give rise to two peaks (spin orbit coupling) in the region of 160–163 eV for thiolates on gold [30], can hardly be seen in the survey spectra. However, in a narrow scan of the S2p region are two peaks seen at 162.1 and 163.2 eV, respectively.

At low take-off angles are the photoelectrons primarily harvested from the SAM/vacuum interface of the sample. The strong gold peaks seen at 90° are therefore dramatically reduced in intensity when approaching 10° . This attenuation is a consequence of the limited inelastic mean free path of electrons in organic materials and the thickness of the densely packed SAM on the gold surface. The O1s peak, on the other hand, shows a significant gain in intensity at near grazing angle, implying a preferential orientation of the SAM with the OEG part exposed to the ambient.

The shorter compounds demonstrate a similar spectral behavior as discussed for $C_{15}EG_6$. It also should be emphasized that no other chemical elements than those discussed for $C_{15}EG_6$ are observed above the noise level in the survey spectra of the investigated SAMs. The spectra recorded at TOA = 10° would be particularly sensitive to the presence of additional elements and contamination on the surface. Thus, the survey spectra confirm that our compounds are of a high purity and that an appropriate protocol is followed during the sample preparation, handling and measurement. Table 2 sum-

Table 2

Binding energies (eV) for core-level electrons detected at TOA = 90° for SAMs formed by $C_{15}EG_{1,2,4,6}$ on gold.

Compound	C1s		O1s		N1s	S2p		
	-C=O	-CH ₂ -O-	-CH ₂ -	-C=O		-CH ₂ -O-		
$C_{15}EG_1$	288.6	286.9	285.1	533.2	531.8	400.5	163.2	162.1
$C_{15}EG_2$	288.5	287.0	285.1	533.4	531.8	400.3	163.2	162.1
$C_{15}EG_4$	288.5	287.0	285.1	533.3	531.8	400.3	163.2	162.1
$C_{15}EG_6$	288.5	287.1	285.3	533.5	531.8	400.4	163.2	162.1

marizes the binding energies of the core level electrons of the OEG SAMs. Distinctive chemical shifts are observed for C1s, O1s, N1s, S2p electrons [31] and they are discussed along with the intensity of the corresponding peaks.

The peaks seen in the C 1s region are due to the presence of three different types of carbon atoms in the SAMs. The narrow scans at TOA = 10° and 90° for all SAMs are compared in Fig. 2. The strong peak with an average binding energy (BE) at 285.2 eV is due to the electrons from the alkyl chains. The binding energy is shifted to 287.0 eV for the electrons originating from the OEG portion of the SAM. Further on, a weak feature is observed at around 288.5 eV that is assigned to C1s electrons from the C=O moiety. Fig. 2 shows a strong correlation between the relative intensities of the peaks and the length of the OEG tails. As expected, the $C_{15}EG_1$ SAM with the shortest tail displays the ether C1s peak with the lowest intensity. Since such a thin oligomer layer gives the smallest attenuation of the electrons coming from the alkyl part of the SAM, the alkyl C1s peak is the strongest one for this SAM. Likewise, the C=O peak is best resolved in the spectra of the $C_{15}EG_1$ SAM. Next, when the oligomer chain length increases, a proportional increase in the intensity of the ether C 1s peak is seen, whereas the alkyl peak decreases as a consequence of a stronger attenuation. Such an intensity behavior previously has been observed for similar OEG-terminated assemblies [1,32] and it reveals that the SAMs are highly oriented, with the OEG portion forming a layer on top of the alkyl underlayer. The orientation of the molecules can be additionally verified by studying the intensity of photoemitted electrons at low take-off angles: the attenuation of the electrons from the interior “bulk” of the SAM increases as compared to those coming from the near SAM/vacuum interface at a low TOA [33–35]. Fig. 2 indeed shows a reduction of the alkyl C1s peak intensity at the expense of the ether and carbonyl C1s peak intensities.

Fig. 2C shows a narrow scan region of the O1s core level electrons. It confirms that two types of oxygen are present in the OEG SAMs. The peak at 533.4 eV is assigned to the ether oxygen, and the weaker one shifted to 531.8 eV is due to the carbonyl oxygen. The intensity of the ether peak increases proportionally to the length of the OEG chain. The N1s electrons (the peak around 400.4 eV, Fig. 3D) also give a similar information about the upright orientation of the molecules in the SAM: they undergo a weaker attenuation by the shorter OEG tails at TOA = 90° and this effect is even more pronounced at TOA = 10° (data not shown).

The S2p electrons due to the sulfur chemisorbed onto Au(111) typically appear in the XPS spectra as a doublet [30] (spin orbit coupling) at 163.2 and 162.1 eV, respectively, Fig. 3. At TOA = 90° are the S2p electrons attenuated proportionally to the thickness of the SAM. A spectrum of 16-mercaptohexadecanol (HS-(CH₂)₁₆-OH) is shown for comparison in Fig. 3. Note that the intensities of the S2p peaks are very similar in the spectra of the alcohol and $C_{15}EG_1$ SAMs. The two SAMs have also comparable thicknesses [10]. If one assumes that the increase in the S2p attenuation due to the amide group and the two methylenes at the terminal portion of $C_{15}EG_1$, as compared one terminal methylene in 16-mercaptohexadecanol, is small, then it can be concluded that the surface coverages for these two SAMs are very similar. How-

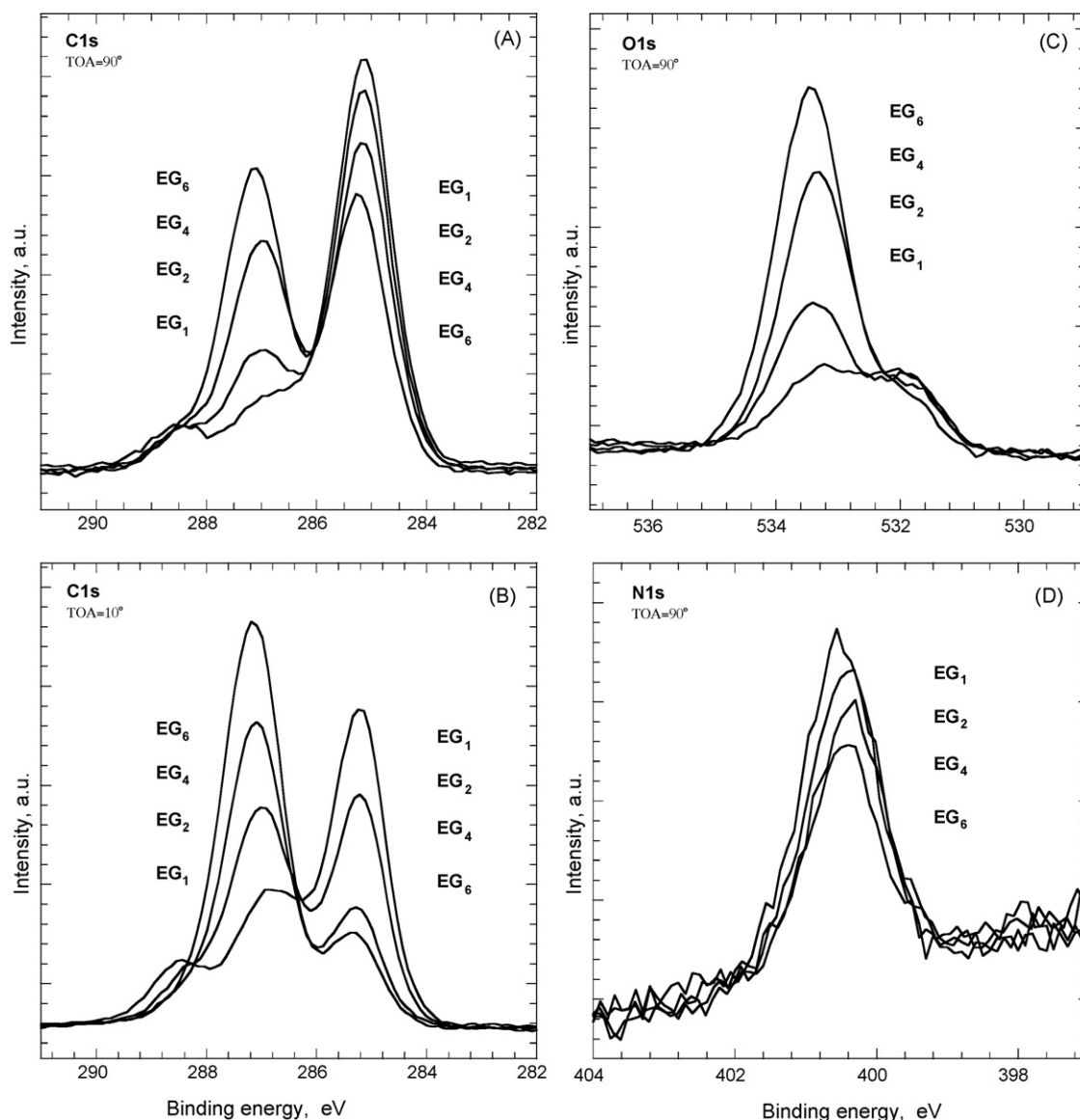


Fig. 2. XPS narrow scan spectra for several OEG-terminated SAMs on gold ($C_{15}EG_n$). A and B show C1s electrons narrow scan spectra of OEG SAMs on gold obtained at two take-off angles, 90° and 10° , respectively. C and D, respectively, show O1s and N1s narrow scan spectra obtained at a take-off angle of 90° .

ever, an exact estimation of the surface coverage for the SAMs of the longer compounds needs an exact account of the attenuation effect.

As expected, the oligomer-dependent attenuation of the S2p electrons is very pronounced at $TOA = 10^\circ$. However, the spectra recorded for $C_{15}EG_6$ reveal two additional broad features at 164 and 169 eV, respectively. The peak at 164 eV previously has been attributed to unbound thiol groups [36]. The oxidation of such groups into SO_x species upon air exposure give rise to a second feature at 169 eV [37]. The fact that the additional features are seen only at $TOA = 10^\circ$ suggests that the unbound and oxidized sulfur species are preferentially located at the SAM/vacuum interface. The unbound thiols and the SO_x species most likely belong to molecules that are interpenetrating the SAM in an upside-down orientation. Another possibility is of course that a small fraction of physisorbed molecules are present on the surface even after extensive rinsing and sonication [38]. The latter suggestion is, however, less likely because no such additional features are seen in the S2p narrow scan spectra of the other SAMs.

Previous studies have shown that it is only the EG_6 chains that adopt the helical conformation at room temperature [10]. Also,

it has to be kept in mind that the compounds interact laterally in SAMs via hydrogen bonds [12,13]. Thus, the overall assembly process relies on a delicate balance between the intra- and inter-molecular interactions and the mass transport from solution. To address this issue in more detail, the $C_{15}EG_6$ SAMs were also prepared from $20 \mu M$ solutions (incubation time was at least 24 h). The C1s, O1s and N1s regions display no significant differences as compared to the samples prepared from mM solutions (data not shown). However, the S2p narrow scan at $TOA = 10^\circ$ shows that the SO_x species are no longer present on the surface of the $C_{15}EG_6$ SAM, Fig. 3.

Although measurements of the ellipsometric thickness showed practically no difference between the $C_{15}EG_6$ SAMs prepared from μM and mM solutions [10,12], respectively, the effect of thiol concentration can be revealed by comparing IRAS data, Fig. 4. The alkyl CH asymmetric and symmetric stretches at 2918 and 2851 cm^{-1} , respectively, confirm that highly ordered all trans alkyl underlayers are present in both SAMs. However, the distinctive peaks due to the helical conformation at 2893 , 1349 , 1244 , 1114 and 964 cm^{-1} gain intensity for the SAM prepared from a μM solution. Thus, an improved crystallinity and/or orientation of the helical EG_6 phase

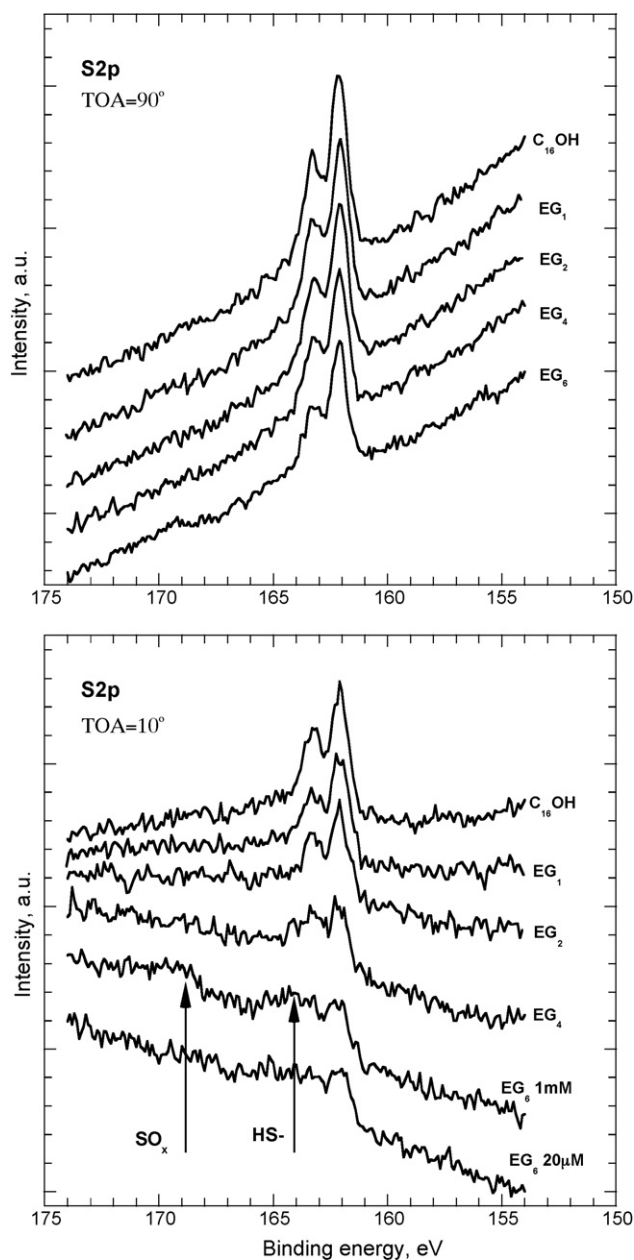


Fig. 3. S2p narrow scan spectra of OEG SAMs on gold obtained at two take-off angles, 90° and 10°.

are clearly visible in the spectra of this SAM when prepared from 20 μM solutions.

The influence of the incubation (adsorption) time on the formation of the C_{15}EG_6 SAM is depicted in Fig. 4C. In this experiment are the IRAS spectra recorded for samples that have been immersed into the 20 μM thiol solutions for 10 min, 24 h and 19 days, respectively. After 10 min incubation the alkyl CH stretches indicate a rather reasonable alignment and packing (2919 and 2851 cm^{-1}). However, the helical EG_6 peaks appear with reduced intensity. Moreover, the presence of the amide I peak at 1649 cm^{-1} (which is not expected to be seen for an ordered assembly, see arrow in Fig. 4C), and the reduced intensity of the amide II peak indicate a poor alignment of the amide group [10]. Thus, the IRAS data shows that long incubation time, at least 24 h, is necessary in order to obtain a highly ordered crystalline EG_6 phase, Fig. 4C. Upon extending the total incubation time to 19 days only small improvements of the crystallinity and/or orientation of the EG_6 portions of the SAM can be

observed, as indicated by the slight increase of the helical OEG related peaks (Fig. 4C). This phase behavior reveals that the self-assembly and the folding of the EG_6 portion into a well-defined helical conformation is a fairly slow process. This is in fact reasonable considering the shape and the relatively large cross sectional area (21.3 \AA^2) of the helix [2]. Note that the packing density of an alkanthiolate SAM adopting a $(\sqrt{3} \times \sqrt{3})\text{R}30^\circ$ overlayer structure on Au(1 1 1) is 21.4 \AA^2 .

Although the XPS data does not indicate any traces of unbound sulfur present in the SAM of C_{15}EG_4 , IRAS measurements reveal that the conformation and/or orientation of the OEG portion depends on the solution concentration. Namely, for an C_{15}EG_4 SAM prepared from a 20 μM solution, Fig. 5, the skeletal COC peak appears at 1148 cm^{-1} , as compared to 1145 cm^{-1} for the same SAM formed in a 1 mM solution [10]. The observed frequency shift along with an increase of the peak intensity points towards an improved packing of the all trans EG_4 phase. However, no effect of a reduced solution concentration and long incubation times is observed for the shortest C_{15}EG_1 and C_{15}EG_2 SAMs.

In figure Fig. 5 IRAS fingerprint signatures of the entire C_{15}EG_n SAMs series ($n = 1, 2, 4, 6, 8, 10, 12$) are compared, including the extended OEG chains, namely C_{15}EG_8 , $\text{C}_{15}\text{EG}_{10}$ and $\text{C}_{15}\text{EG}_{12}$. Even in these SAMs, which were prepared from 20 μM solutions, the OEG portion adopts the helical conformation as confirmed by the increasing intensity of the helical OEG-related peaks. Moreover, Svedhem et al. showed in their previous work using null ellipsometry that the incremental increase in thickness (2.8 \AA) for these SAMs was in agreement with the number of units in the OEG chain [27]. Importantly, at the same time the constant portion ($-\text{S}(\text{CH}_2)_{15}\text{CONH}-$) of the entire OEG-terminated SAM series is isostructural, as confirmed by the distinctive amide IRAS fingerprint in the low frequency region (Fig. 5) and by the alkyl asymmetric and symmetric CH_2 stretched at 2918 and 2851 cm^{-1} , respectively (not shown).

3.2. Influence of supporting alkyl layer on the OEG SAM order and conformation

To address the importance of the supporting alkyl layer for the structure of the OEG-terminated SAMs, we also compared assemblies formed by $\text{HS}(\text{CH}_2)_m\text{CONH}-(\text{CH}_2\text{CH}_2\text{O})_n\text{H}$, where $m = 2, 5, 11$, and $n = 4, 6$ [10,27]. Previous investigators have reported on chain length-dependent structural variations of alkanthiolate SAMs [39–41]. Furthermore, Vanderah et al. [20,21] showed that SAMs formed by a series of compounds $\text{HS}-(\text{CH}_2\text{CH}_2\text{O})_n\text{CH}_3$ displayed a remarkable conformational uniformity, i.e., the OEG portion adopted a distinctive helical conformation even without the supporting alkyl layer. Therefore, it would be interesting to investigate how critical the length of the supporting alkyl layer is for the assembly of amide-containing OEG SAMs. As mentioned before, we introduced the lateral hydrogen bonds in these SAMs to improve their stability, an issue, which has proven crucial when fabricating biosensor interfaces [42] and SAM-based nanoarchitectures [43].

Fig. 6 shows the CH stretching and fingerprint regions of IRAS signatures of a series of SAMs, C_mEG_n with lengths of the supporting alkyl portion being $m = 2, 5, 11$ and 15, respectively, and the OEG portion being $n = 4$ and 6. The results for the $m = 11$ and 15 series have been discussed extensively in our previous studies [12,13]. They allowed us to conclude that the terminal portions of the SAMs have nearly identical structures (all trans for EG_4 and helical for EG_6 , respectively) independently of the alkyl chain length. However, the IR signatures of the $m = 2, 5$ series display substantial structural differences. The general trend is that the intensities of the “helical” peaks of the EG_6 -terminated SAMs, in particular the COC stretching peak at around 1114 cm^{-1} , have decreased significantly. The COC peak corresponding to the all trans EG_4 conformation also appears

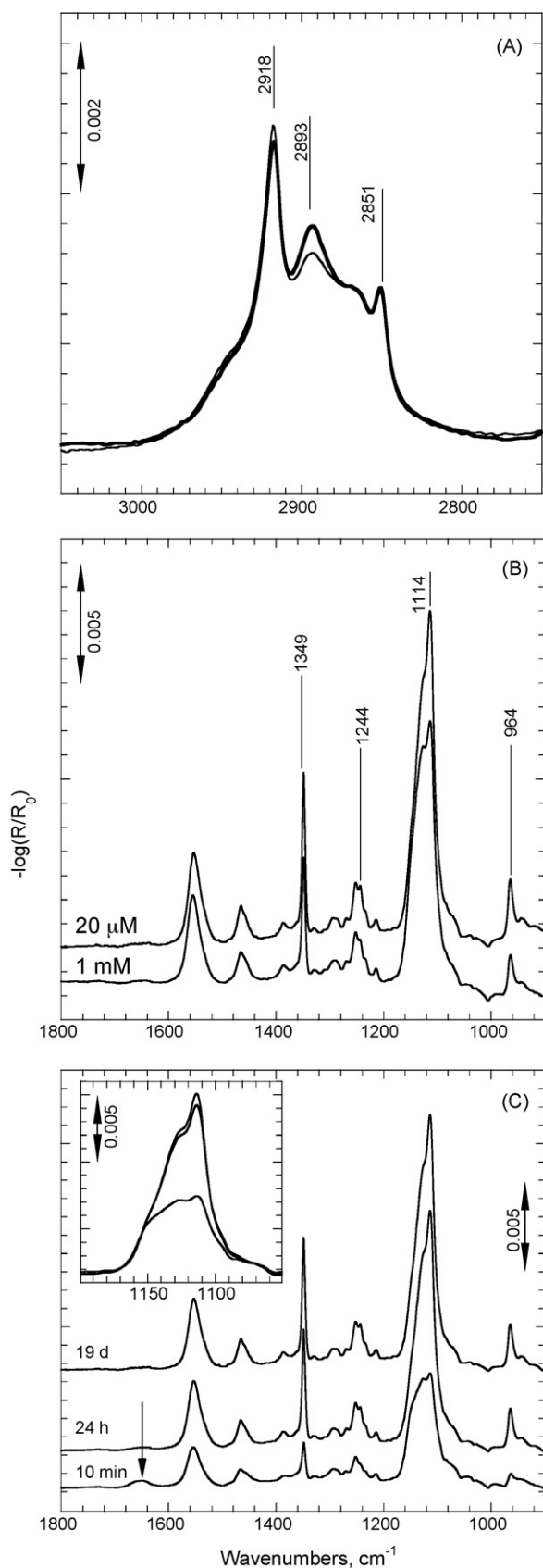


Fig. 4. Infrared reflection-absorption spectra (IRAS) of the $C_{15}EG_6$ SAM in the CH stretch region (A) and fingerprint region (B). In A corresponds the thick line to the spectrum of the SAM formed from a $20\ \mu\text{M}$ solution and the thin line from a $1\ \text{mM}$ solution. Panel C shows spectra of $C_{15}EG_6$ SAMs prepared from a $20\ \mu\text{M}$ solution for 10 min, 24 h and 19 days, respectively. The inset enlarges the $1200\text{--}1050\ \text{cm}^{-1}$

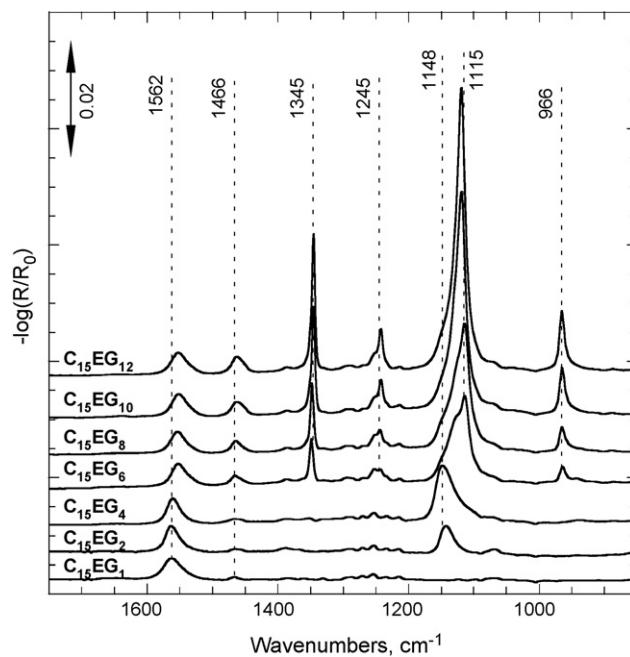


Fig. 5. Fingerprint region of infrared reflection-absorption spectra obtained for oligo(ethylene glycol)-terminated self-assembled monolayers (SAMs) on gold. The SAMs were formed from $20\ \mu\text{M}$ solution of compounds with the general structure $\text{HS}(\text{CH}_2)_{15}\text{CONH}-(\text{CH}_2\text{CH}_2\text{O})_n\text{H}$, where $n = 1, 2, 4, 6, 8, 10, 12$.

with reduced intensity, in particular for C_2EG_4 . For the latter SAM, a significant change is also observed in the CH region (Fig. 6). Note, that the amide I and II peaks at around 1650 and $1550\ \text{cm}^{-1}$ are informative for structural changes in this class of SAMs. For example, amide I peak appears for C_2EG_4 , at the same time as amide II peak is decreased and red-shifted by $\sim 9\ \text{cm}^{-1}$ for C_2EG_4 and C_5EG_4 SAMs as compared to the $C_{11}EG_4$ and $C_{15}EG_4$ SAMs. The decrease of the amide II peak is also seen for the C_2EG_6 and C_5EG_6 SAMs.

Taken together, the IR observations suggest that the shorter supporting alkyl chain, $m = 2, 5$, has a negative effect on the packing, orientation and conformation of the OEG-terminated, amide-containing SAMs. The presence of the amide linkage in the constituent molecules affects the structure of the resulting assembly, a clear difference from the HS-EG_x SAMs reported by Vanderah et al. [20,21]. Interestingly, for the C_2 supported SAMs the degree of disorder seems to be higher than for the C_5 supported analogs, a behavior, which might suggest a contribution of the odd-even effect [41]. Although we have not synthesized analogous compounds to verify if the critical alkyl length to achieve an ordered SAM is C_{11} , our experiments clearly point out that a long-chain alkyl supporting layer is critical for obtaining highly ordered OEG SAMs stabilized by the amide hydrogen bonds. One possible explanation could be that the formation of a lateral hydrogen bonding network introduced between the alkyl and OEG portions of the SAM has to be defined by a robust template of strongly interacting alkyls, and not vice versa. This condition is certainly fulfilled in C_mEG_n SAMs with $m \geq 11$. The tendency to form ill-defined SAMs when the supporting alkyl is short, also could be related to differences in the assembly kinetics. Detailed quantitative investigation of these effects is beyond the scope of this paper, but the performed comparison of the C_mEG_n SAM series clearly suggests that subtle changes in chain length can have a huge impact on the structure of the resulting SAMs.

region where the skeletal COC stretching modes absorb. The arrow identifies the Amide I peak in the spectrum obtained after 10 min incubation. See text for further details.

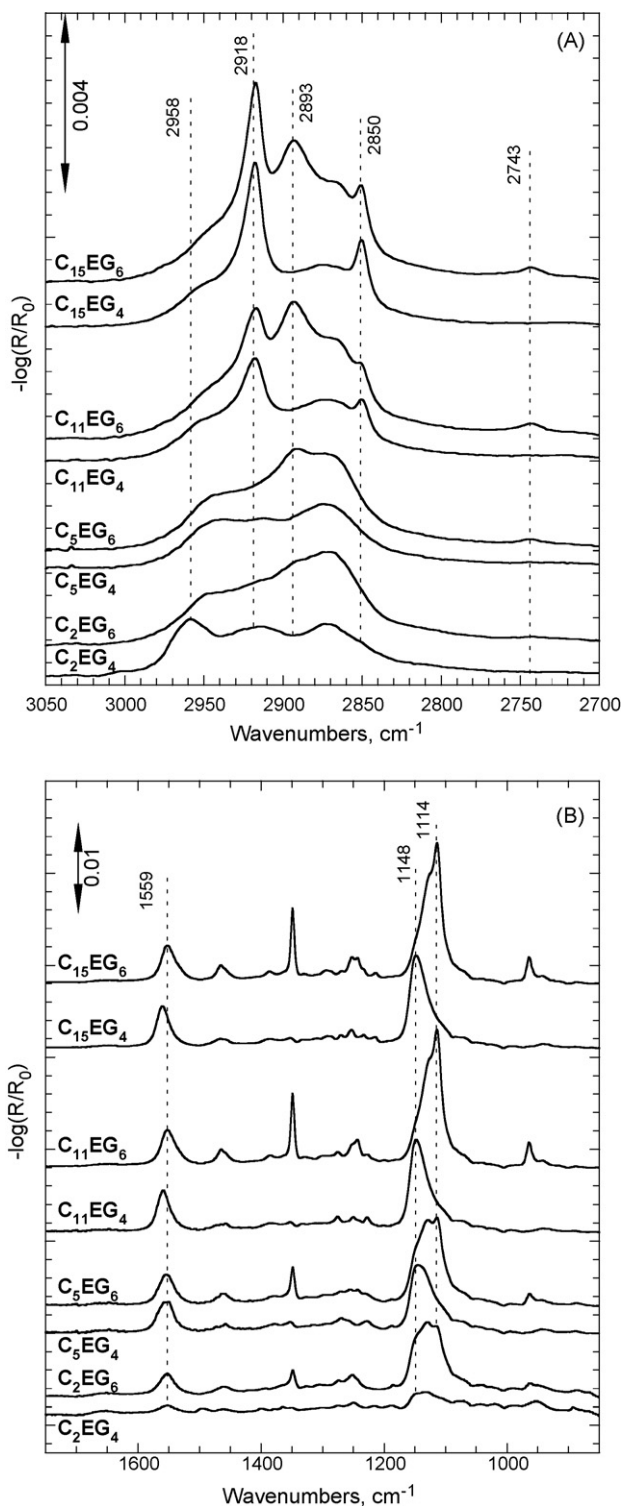


Fig. 6. Infrared reflection-absorption spectra in the CH and fingerprint regions of a series of SAMs on gold with the general structure $-S-(CH_2)_m-CONH-(CH_2CH_2O)_nH$, where $m = 2, 5, 11, 15$ and $n = 4$ or 6 .

3.3. Structure and orientation of the OEG-terminated SAMs as inferred by *ab initio* modeling

Infrared RA spectroscopy has revealed a rich conformational and phase variation of OEG-terminated SAMs composed of amide-bridged alkyl and OEG portions of different lengths. Many of the observed spectral peculiarities are different from the OEG-

containing systems reported and developed by other groups [1,2,8,20,21]. Therefore, a comprehensive understanding of the fundamental origin of subtle spectral details is crucial for full exploration of their potential in the field of nanomaterials and nanodevices. The essential questions one has to answer when analyzing the IRAS data are (i) assignments of the spectral peaks, (ii) orientation of the structural blocks of the molecules in the SAM, (iii) defect structure and phase behavior. As we will demonstrate later, based on this solid knowledge it is possible to design completely new assemblies offering a promising platform for construction of advanced molecular architectures.

To address the above questions, we have conducted a wide scale *ab initio* modeling of infrared RA spectroscopy data in two frequency regions, the fingerprint region with the amide region included ($900-1800\text{ cm}^{-1}$) and the CH_2 -stretching region ($2800-3000\text{ cm}^{-1}$), respectively. The former is dominated by the OEG optical response, whereas the latter is contributed by both alkyl and OEG moieties. The vibrational spectra of both molecular constituents are well understood [44–47]. However, for SAMs on metal substrate, the selection rule of reflective surface makes the apparent IR absorption spectrum strongly dependent on the molecular orientation. Therefore, to rationalize the shape and intensity of characteristic peaks in the fingerprint region, one needs to know the values of tilt and twist angles of the OEG portion within the SAM. The in-SAM orientation of alkyl, amide, and OEG is required to understand the CH_2 -stretching region, as well as more subtle spectral details which are due to collective modes. In general terms, the molecular orientation is a reflection of the SAM interior determined by specific intra- and inter-molecular interactions between SAM structural components. Its quantitative evaluation is thus the principal task for the theoretical modeling.

Here, we examine the in-SAM molecular orientation in the context of its spectral appearance, likely intra-molecular defects, and formation of hydrogen bonding. Our analysis is based on all-electrons *ab initio* calculations of molecular geometry, vibrational frequencies, and transition dipole moments.

We adopt the following methodology for calculations. The spectrum of molecular self-assembly can be described by a combination of Gaussian/Lorentzian-shaped peaks whose position, width, and intensity are fully or partly taken from the experiment [48]. We found it sufficient to represent the absorbance of SAMs in focus by the sum of Lorentz-type curves

$$A(\nu) \sim \sum_i \frac{(\mu_{\perp}^{(i)})^2}{(\nu - \nu_i)^2 + \sigma_i^2}, \quad (1)$$

where each peak is centered at the frequency ν_i and has the half width at half maximum (hwhm) σ_i , $\mu_{\perp}^{(i)}$ represents the component of the transition dipole moment (TDM), perpendicular to the metal surface. For TDMs associated with vibrations of the alkyl moiety,

$$\mu_{\perp}^{(i)} = -\mu_x^{(i)} \sin \theta_A \cos \psi_A + \mu_y^{(i)} \sin \theta_A \sin \psi_A + \mu_z^{(i)} \cos \theta_A, \quad (2)$$

where θ_A and ψ_A are the tilt and twist angles of alkyl CCC plane, as defined in Ref. [48]. In these equations, σ_i , θ_A , and ψ_A are considered as adjustable parameters. We have used one or, at maximum, two best-fit values of σ_i . Finding the molecular orientation angles from the comparison of observed and calculated spectra is described in Ref. [15]. The frequencies ν_i of the normal modes and respective TDMs μ^i were calculated *ab initio* with the BP86 exchange-correlation functional, basis set 6-31G* (or larger for cross-checking). The contributions into the observed IRA spectrum from OEG and amide portions were obtained in a similar way. The required Euler angles $\{\theta_E, \psi_E\}$ and $\{\theta_N, \psi_N\}$ were calculated for the *ab initio* found molecular geometry and given values of $\{\theta_A, \psi_A\}$.

Table 3
Likely orientation of the alkyl chain (θ_A , ψ_A , and φ_A) in SAMs of HS(CH₂)₁₅CONH–EG₆, where the OEG moiety can be in helical (H) and all trans (T) conformations [10,12]. The Euler angles which determine in-SAM orientation of the OEG (θ_E , ψ_E , and φ_E) and amide (θ_N , ψ_N , and φ_N) are calculated for the optimized geometries of H and T conformations of SAM constituents. Calculation details are described in Ref. [15].

	θ_A	ψ_A	φ_A	θ_E	ψ_E	φ_E	θ_N	ψ_N	φ_N	Calculated (measured) thickness (Å)	H···O bond length (Å)
H	26°	–62°	–77°	22°	24.5°	–151°	–27°	–4°	–3°	38.9 (39.8) ^a	2.6
T	26°	65°	82°	33°	41°	74°	34°	4°	0°	40.6 (n.a.)	2.2

^a Experimental accuracy about 1.7 Å [12].

According to Eqs. (1) and (2), the SAM spectrum is independent of the third Euler angle, the azimuthal angle φ_A . However, the presence of amide bridge imposes additional constraints on the orientation of molecules within the SAM. Earlier, we have reported experimental evidences, clearly indicating the formation of a network of lateral hydrogen bonds [12,13]. This implies some favorable orientation of alkyl and OEG parts. Therefore, θ_A and ψ_A are to be adjusted together with φ_A in a way providing the minimal possible H···O distance between the neighboring amide groups. To notice, in a perfect arrangement of molecules HS(CH₂)_mCONH–EG_n which repeats the hexagonal ($\sqrt{3} \times \sqrt{3}$) R30° structure of the Au(111) surface, this minimal H···O distance is noticeably larger, than the typical length of a hydrogen bond H···O.

The optimization of molecular geometry for molecules HS(CH₂)_mCONH–EG_n with different *m* and *n* and calculations of entries in the absorbance were performed using several methods and different basis sets to ensure objectiveness of the obtained results. The DFT method BP86 with 6-31G* basis set was identified as optimal for this modeling in terms of both, reasonable time and good agreement with the experiment. We did not scale frequencies or/and intensities of OEG characteristic peaks. In all calculations, we have used the Gaussian-03 package of programs.

By using ab initio calculated optimized geometry and TDMs of vibrational modes, we can find the molecular orientation and determine the peak assignments. The averaged orientation of alkyl chains within the SAM, which is deduced from the comparison of experimental and model IR RA spectra, and the Euler angles for amide and OEG portions dictated by the optimized geometry of C₁₅EG₆ in helical (H) and trans (T) conformations are represented in Table 3. These data refer to the spectra of one and the same SAM but measured at room and ~60 °C temperatures, at which the spectral signatures of H and T conformations, respectively, are well documented [10,12]. The orientation angles, which differ from those listed in Table 3 by less than ±5°, give nearly the same agreement between the calculated and experimental spectra, whereas large deviations, particularly, in values of θ_A , lead to increasing divergences between this modeling and experiment. The main directing angle is thus

set into a range 20° < θ_A < 30°. In alkanethiolate SAMs terminated with OH [49,50] and OEG [2] groups, the θ_A was reported to be about 30°. Thus, our result is in agreement with the reported data, suggesting that the introduction of the –CONH–EG₆ terminus does not affect strongly the tilt of alkyl chains. However, it should be noticed that the mentioned similarity of alkanethiolate SAMs with different terminal groups does not resolve the controversy between the above-quoted IR spectroscopy data and NEXAFS measurements which gave a noticeably larger alkyl tilt angle in OH-terminated alkanethiolate SAMs [51,52].

Fig. 7 compares the observed and calculated spectra in the fingerprint region, and Table 4 specifies the observed and calculated frequencies and their assignments. As seen, the positions and relative intensities of almost all characteristic peaks in the model spectra are in a very good agreement with the experiment. We consider this coincidence as the major proof of the likely molecular orientation in SAMs of this type. In addition, this orientation gives the SAM thickness which is very close to the experimental value, and the obtained H···O length (Table 3, not optimized) is consistent with the formation of lateral hydrogen bonding. Similar calculations for SAMs, which have different length of only alkyl, only OEG, or both alkyl and OEG parts, led us to the conclusion that on the average the alkyl CCC plane is tilted by $\theta_A \sim 26^\circ$, rotated about the substrate normal by $\varphi_A \sim 80^\circ \pm n60^\circ$, and twisted within the range of $\psi_A = -65^\circ$ to -58° [15,17].

The calculations illustrated in Fig. 7 explain the experimentally observed disappearance of wagging and rocking vibrations in the trans conformation of OEG SAMs [12] by the substantial decrease of TDM values under the helical–trans phase transition (see Ref. [16] for more details). The interpretation of other peaks, except the peak dominating the region, is similar to previously reported findings [2,10,12]. Later on, we shall discuss the apparently complex structure of COC peak at ~1100–1150 cm^{–1}, as an illustration of improved understanding of peak assignments.

It should be noticed that studies of ethylene–glycol spectra go back to the pioneering GF-matrix investigation of poly(ethylene–glycol) normal vibrations by Miyazawa et al. [45–47] As admitted in these early publications, the assignment of the peak

Table 4
Measured [12] and calculated frequencies (in cm^{–1}) and their assignments for a C₁₅EG₆ SAM.

H observed	H calculated	T observed	T calculated	Assignment
964	947	–	–	CH ₂ rocking and asym.
~1050	1079	~1060	1058	C–O–C stretching CH ₂ rocking and asym. C–O–C stretching
1114	1111	1144	1140	asym. C–O–C stretching
1243	1214, 1224, 1290	1243	1289	CH ₂ twisting
1252	1223, 1233	1253	1220.5, 1273	amide III ^a
1349	1336	–	–	CH ₂ wagging
1464	1467	~1465	1498	CH ₂ bending
1553	1555	1559	1559	amide II
2851	2950	2851	2949	alkyl CH ₂ sym. stretching
~2864	2891	Broad ^b	2912	OEG CH ₂ sym. stretching
~2892	2925	Broad	2947	OEG CH ₂ asym. stretching
2918	3003	2918	3003	alkyl CH ₂ asym. stretching

^a A scaling factor of 1.037 was used only for amide II, III frequencies.

^b "Broad": a broad peak seen between the alkyl symmetric and asymmetric peaks [12].

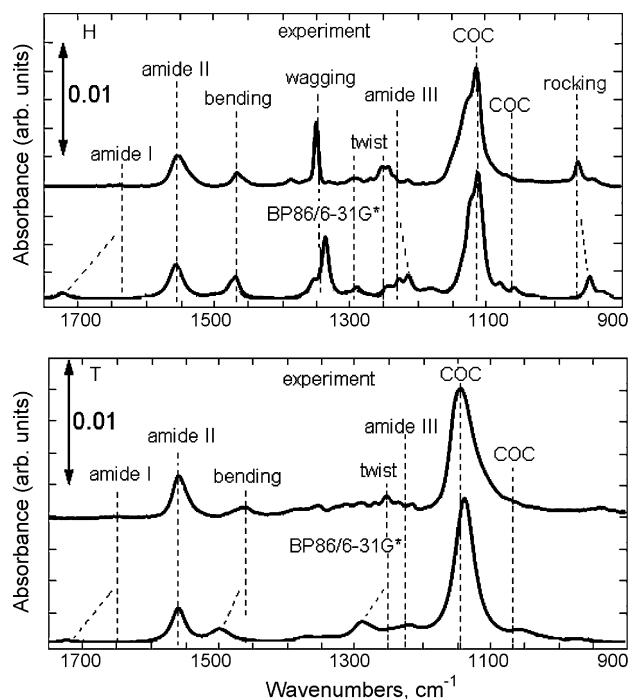


Fig. 7. Observed and calculated spectra for SAMs of $C_{15}EG_6$ molecules in helical and all trans conformations. hwhm = 6 and 12 cm^{-1} for OEG and amide peaks, respectively.

near 2890 cm^{-1} to CH_2 stretching symmetric vibrations was controversial. In fact, the ab initio analysis of vibrational modes clearly shows that the OEG peak, dominating the CH_2 -stretching region (not shown) has to be attributed almost exclusively to asymmetric vibrations [14,16].

The above discussion raises the question: are the molecular orientation and equilibrium geometry obtained at the single-molecule level consistent with the in-SAM molecular environment and to what extent? We have tried to answer this question by modeling periodic molecular arrays at the ab initio level. This kind of the all-electrons first-principle calculations for molecules as large as $C_{15}EG_6$ is not practical. Therefore, we optimized the hexagonal periodic structure of molecules $C_3\text{CONH-EG}_3$. These calculations have been performed with the initial geometry and orientation, as described above, by using the BP86 exchange correlation functional with 6-31G basis set. In brief (details are described elsewhere [26]), it is shown that “switching on” the intermolecular interaction changes the orientation of all three structural components, alkyl, amide, and OEG. However, this effect has minor reflections in the appearance of the model SAM spectrum because TDM z-components of all characteristic vibrations in the fingerprint region are substantially larger than the other. Hence, the Euler angles in Table 3 can be utilized for estimating the molecular orientation.

The comparison of the initial and optimized geometries of periodic arrays showed that the adjustment of individual molecules to the SAM environment is driven towards the formation of lateral hydrogen bonds. As a result, the initial $\text{H}\cdots\text{O}$ distance, 2.6 and 2.5 \AA for helical and all trans OEG conformers, respectively, adopts the equilibrium values 1.91 and 1.87 \AA , respectively. It is worth noting that the calculated length of hydrogen bonding in $C_3\text{CONH-EG}_3$ periodic arrays is shorter for the all trans conformation, in agreement with experimental estimates [12].

In many experimental studies, attention has been paid to the nontrivial structure of COC peak near 1100 cm^{-1} . The pronounced high frequency shoulder observed in hydrogen terminated OEG

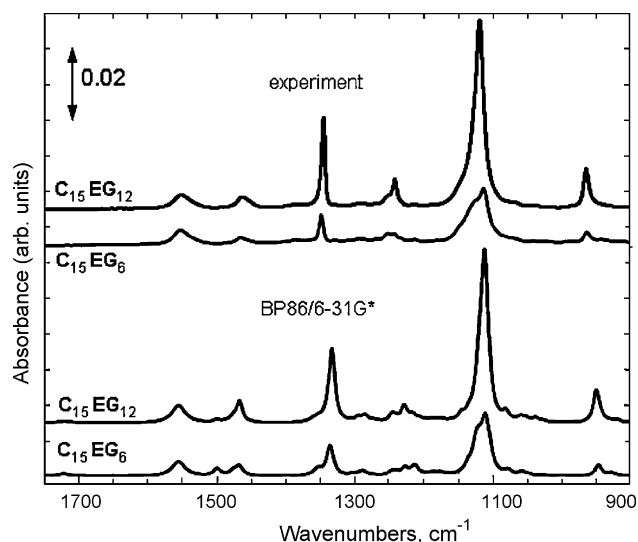


Fig. 8. Observed and calculated spectra for $C_{15}EG_6$ and $C_{15}EG_{12}$ SAMs. In the calculated spectra: hwhm = 6 cm^{-1} (EG_6) and 5 cm^{-1} (EG_{12}) for OEG peaks; hwhm = 12 cm^{-1} for amide peaks; orientation angles of the alkyl chain $\theta_A = 26^\circ$ and $\psi_A = -62^\circ$ are the same for both molecules.

SAMs was often attributed to the presence of gauche defects [2,11]. This type of defects, if close to the SAM/ambient surface, was considered as potential water binders [53]. We have evaluated the possible role of gauche–trans defects on the shape of COC peak by calculating IR absorbance spectra for different OEG conformers [18]. As known from the experiment, the spectral appearance is dependent on the SAM terminal group. Furthermore, the COC peak has different shape in SAMs with different linkage groups (e.g., ether or ester) between alkyl and OEG. The role of these factors in the COC peak formation must be discriminated from the effects caused by the presence of defects. This has been accomplished in the case of simple self-assemblies of $\text{HS-(CH}_2\text{CH}_2\text{O)}_{5,6}\text{-CH}_3$ studied experimentally by Vanderah et al. [3]. As shown in Ref. [18], the COC peak shape is mostly governed by the contributions from different modes of skeletal vibrations of an all helix OEG chain. Nearly full agreement with the experiment is achieved for SAMs modeled as a mixture of host (helical) and guest (all trans) molecules in proportion $\sim 97\%$ to 3% . This is an interesting observation that rules out the presence of helical conformers with single trans and/or gauche defects in the OEG moiety (at least, in the amount affecting the apparent RA spectra).

In SAMs containing amide bridged alkyl and OEG portions, the nature of COC peak is more complicated. In particular, our calculations show that the high-frequency shoulder in the spectrum of the $C_{15}EG_6$ molecule should be understood as a signature of coupled amide–OEG vibrations, and not as normal modes of the OEG chain. This coupling strongly enhances the COC–peak shoulder, which is characteristic for hydrogen-terminated, but not for methyl-terminated OEG SAMs. The series of SAM spectra obtained for different lengths of alkyl chains show only minor, practically negligible effects on the COC–peak shape. We found that to agree the model calculations with the experiment, defects in the form of all trans conformers have to be admitted. We estimate their amount fall in the range around 5–10% even in the best samples. Hence, the above mentioned alternative interpretation of the high-frequency shoulder of COC peak in terms of a disordered OEG tail composed of conformers with gauche/trans defects seems very unlikely.

In the observed spectra of SAMs containing extended ($m > 6$) OEG chains, the asymmetry of the COC peak decreases, see Fig. 8. For $m = 12$ the peak dominating the fingerprint region has no

shoulder at all. Comparison of calculated spectra for $C_{15}EG_6$ and $C_{15}EG_{12}$ molecules exhibits the same trend. In this figure we present the observed (upper panel) and calculated (lower panel) spectra of HSC₁₅CONH-EG_{*n*} molecules. The alkyl portion of both molecules has the same orientation: $\theta_A = 26^\circ$, $\psi_A = -62^\circ$. As seen, all peaks observed in this region are well reproduced in the calculated spectra. The relation between the integrated intensities of the dominant peak for $n = 12$ and $n = 6$ is close to two, which is consistent with the corresponding relation for measured spectra. For the orientation parameters used, the calculated SAM thickness (~ 53 Å) is somewhat lower than the measured value [27] (56 ± 0.4 Å), which is within the accuracy of this modeling. This comparison of experimental observations with theoretical predictions reconfirms the predominantly multimode nature of the COC peak and that it is affected, as discussed above, by three major factors: (i) the OEG end group, (ii) amide bridge, and (iii) the presence of small portion of all trans defects. With an increase of OEG length, the role of the first two factors becomes negligible. The nearly perfect symmetry of the observed COC peak in SAMs with longer OEG termini and nearly perfect reproduction of the observed peak shapes by model spectra provides convincing evidence of a low concentration of all trans defects, i.e., an improvement of quality in SAMs containing longer OEG chains.

3.4. Influence of an additional amide and alkyl layer

The unique structural and phase properties of the OEG-terminated and hydrogen-bonded SAMs encouraged us to explore possibilities for a “modular approach” in assembling even more complex molecular architectures. Namely, we increased the complexity of $C_{15}EG_6$ by synthesizing an extended alkyl chain analog $C_{15}EG_6C_{16}$ [22,27]. Surprisingly, this compound formed a highly ordered, in plane stabilized SAM, with IR characteristics, which previously could be observed only for conformationally frozen long alkyl SAMs at low temperatures and for highly crystalline polymethylenes [54]. As seen from Fig. 9, the distinctive all trans alkyl and helical OEG-related IR signatures of the $C_{15}EG_6C_{16}$ SAM show the general tendency of increasing intensity as compared to those seen in the $C_{15}EG_6$ SAM spectra. Moreover, the asymmetric methyl stretch appears at the CH region as a doublet at around 2963 and 2956 cm^{-1} , respectively.

To rationalize the effect of the extended terminal alkyl chain on the structure of the $C_{15}EG_6C_{16}$ SAM we also synthesized a shorter analog $C_{15}EG_6C_1$, Fig. 9. Interestingly, the fingerprint region of the SAMs with the C_1 and C_{16} termini looks identical. This observation strongly suggests that the EG_6 portion is highly ordered and in-plane stabilized by the two sheets of lateral hydrogen bonds (see the structure of the compounds in Table 1) and that the length of the terminal alkyl has a minor effect on the OEG conformation. Such an interpretation is further supported by the fact that the amide I signature is absent in both RA spectra, whereas the amide II peak is at exactly the same position (1551 cm^{-1}) and has similar intensity for both SAMs.

As shown, the precise knowledge of in-SAM molecular orientation requires the understanding of the interrelation between the SAM structure and IR spectrum. With the increase of SAM complexity, e.g., $C_{15}EG_6 \rightarrow C_{15}EG_6C_{16}$ the number of “influential” orientation parameters is nearly doubled that makes the establishment of a structure–spectrum relationship much more complicated. Fig. 10 illustrates BP86 optimized geometries of typical SAM constituents with two alkyl chains which are coupled to the central OEG part via amide bridges. Sulfur atoms form the $(\sqrt{3} \times \sqrt{3}) R30^\circ$ lattice and tilt of the lower alkyl was chosen so as to reproduce the measured SAM thicknesses. Details of these model structures and their relevance to the real self-assemblies will be discussed elsewhere. Here we just want to draw attention to the structural effects of

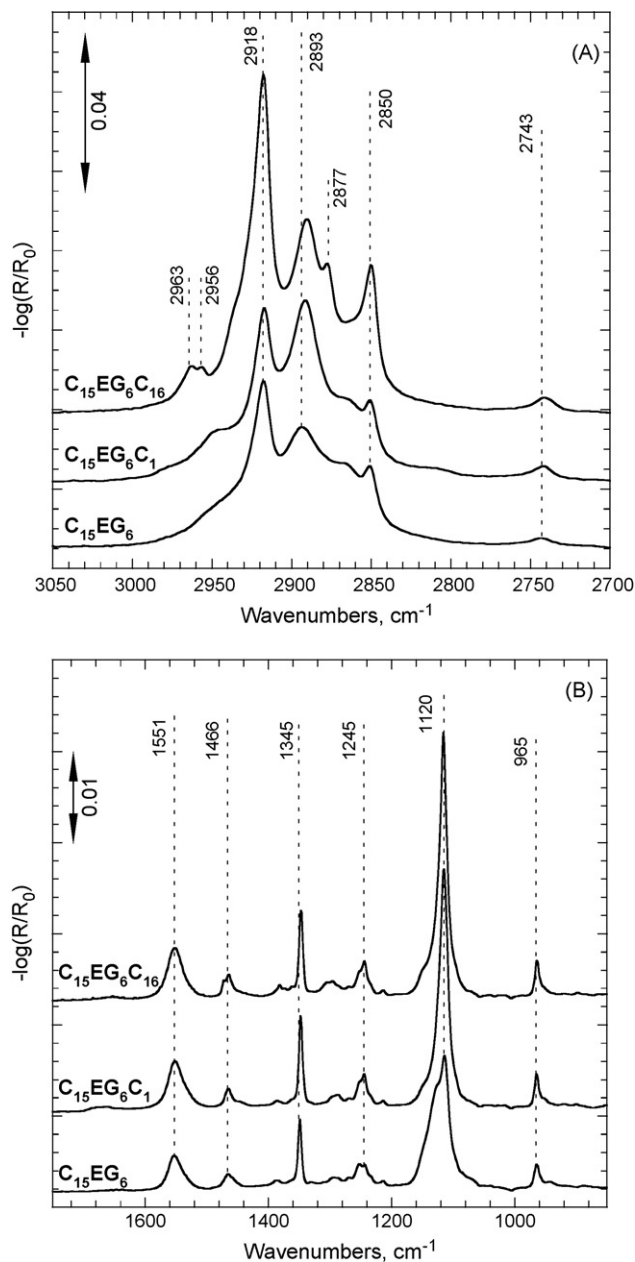


Fig. 9. Infrared reflection–absorption spectra in the CH and fingerprint regions of SAMs on gold formed by two extended alkyl chain OEG compounds, $C_{15}EG_6C_1$ and $C_{15}EG_6C_{16}$, compared to $C_{15}EG_6$.

the attachment of an additional amide–alkyl module to the OEG-terminated SAMs. First, the upper alkyl chain does not repeat the orientation of the lower one. Second, the characteristic tilt θ_E of the OEG helix adopts a noticeably smaller value in comparison with OEG SAMs having one alkyl layer. Third, the orientation parameters of the end methyl group in $C_{15}EG_6C_1$ and $C_{15}EG_6C_{16}$ are substantially different as compared to C_1 and C_{16} SAMs, respectively. For example, according to our modeling, if the lower alkyl chain C_{15} is tilted by $\theta_A = 26^\circ$ and rotated by $\psi_A = -62^\circ$, the tilt angle of the upper C–C bond in HS(CH₂)₁₅–CH₃ and $C_{15}EG_6C_{16}$ molecules differs by about 30° . These and other peculiarities of the molecular orientation in alkyl–OEG–alkyl SAMs are expected to have certain signatures in the RA spectra to be examined in the nearest future.

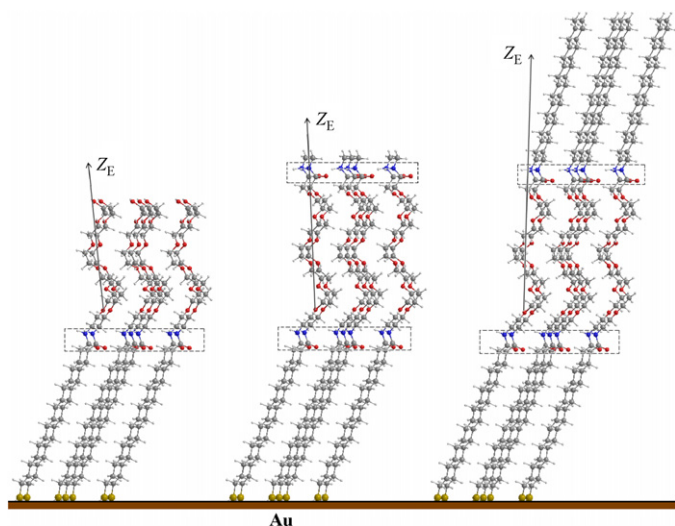


Fig. 10. BP86/6-31G* optimized geometries of periodic arrays of $C_{15}EG_6$ (left), $C_{15}EG_6C_1$ (middle) and $C_{15}EG_6C_{16}$ (right) molecules on gold. The molecules are arranged in a hexagonal ($\sqrt{3} \times \sqrt{3}$)R30° lattice with the sulfur–sulfur separation 5 Å. The OEG axes are denoted by Z_E . Orientation of the alkyl chain is $\theta_A = 26^\circ$, $\psi_A = -62^\circ$ and $\varphi_A = 0$ for all molecules. Dashed frames indicate the position of the lower and upper amide groups, respectively.

4. Conclusions and outlook

We have studied experimentally and theoretically the quality, conformation, defect structure and IR signatures of a library of OEG-containing SAMs. The particular set of SAMs enabled us to address several critical issues of relevance to the self-assembly of highly ordered and stable structures consisting of entities more complex than those formed by simple ω -substituted alkylthiols on gold. For example, we found that the preparation conditions are crucial in order to avoid defects existing in a form of upside-down oriented thiol compounds in a SAM formed by $C_{15}EG_6$. While it is difficult to recognize these preparation-related defect signatures and to make unambiguous interpretation of the IRAS data, XPS strongly suggests that compounds with structurally complex tails as the helical OEG should be prepared keeping the incubation solution concentrations as low as possible (typically $\sim 20 \mu\text{M}$). Further on, the supporting alkyl chain length is critical for obtaining ordered structures for the present set of OEG SAMs containing amide linking groups. For example, EG_4 and EG_6 -terminated SAMs appeared disordered for C_2 and C_5 chain lengths, but when C_{11} and C_{15} were employed as a spacer the corresponding SAMs displayed distinctive all trans and helical IR signatures, respectively. This points on the role of the van der Waals interactions between the supporting methylenes, which are known to be critical when matching the alkylthiolate overlayer with the Au(111) crystal face. Also, we have shown that once this condition is fulfilled, the length of the terminal OEG chain can be varied from EG_1 to, at least, EG_{12} without compromising the structural integrity of the SAMs.

Our work also points out on the importance of the choice of appropriate modeling tools to understand the huge variety of spectral peculiarities in the infrared signatures of the OEG-containing SAMs. Previously we demonstrated that molecular orientation and equilibrium geometry obtained at the single-molecule level gives a satisfactory agreement with experimental data. This approach enabled us to identify the contributions from different skeletal COC modes, all trans defects, and the amide coupling group to the strongly asymmetric appearance of the COC peak of helical OEG SAMs.

Finally, a modular approach to the synthesis of analogs combined with DFT calculations enabled us to obtain a deeper insight

into the origin of unique structural properties of the extended alkyl SAMs such as those formed by $C_{15}EG_6C_{16}$. The obtained BP86 optimized geometries revealed that the two alkyl chains within these SAMs are likely oriented differently as compared to the OEG-terminated SAMs without the extended alkyl chain and simple alkylthiolate SAMs, respectively. The infrared RA spectrum of $C_{15}EG_6C_1$ confirmed that the orientation of the helical EG_6 portion is primarily affected by the second hydrogen bond (amide) layer rather than the extended alkyl portion. The reported finding outlines a route for synthesis of a new generation of highly ordered, stable and relatively thick SAMs which are based on alkyl and OEG modules interlinked by amide bridges. In our forthcoming publications we will provide more details about the structure of these unique self-assembling compounds and will demonstrate their potential in nanoscience and nanotechnology.

Acknowledgments

This work was supported by the Swedish Foundation for Strategic Research (SSF) through Graduate School Forum Scientium and Biomics program. This work is also supported by the Swedish Research Council (VR), the Swedish Institute through the Visby program and Lithuanian State Science and Studies Foundation.

References

- [1] C. Pale-Grosdemange, E.S. Simon, K.L. Prime, G.M. Whitesides, *J. Am. Chem. Soc.* 113 (1991) 12–20.
- [2] P. Harder, M. Grunze, R. Dahint, G.M. Whitesides, P.E. Laibinis, *J. Phys. Chem. B* 102 (1998) 426–436.
- [3] D.J. Vanderah, J. Arsenault, H. La, R.S. Gates, V. Silin, C.W. Meuse, G. Valincius, *Langmuir* 19 (2003) 3752–3756.
- [4] D.J. Vanderah, H.L. La, J. Naff, V. Silin, K.A. Rubinson, *J. Am. Chem. Soc.* 126 (2004) 13639–13641.
- [5] S. Herrwerth, W. Eck, S. Reinhardt, M. Grunze, *J. Am. Chem. Soc.* 125 (2003) 9359–9366.
- [6] D. Schwendel, T. Hayashi, R. Dahint, A. Pertsin, M. Grunze, R. Steitz, F. Schreiber, *Langmuir* 19 (2003) 2284–2293.
- [7] M.W.A. Skoda, R.M.J. Jacobs, J. Willis, F. Schreiber, *Langmuir* 23 (2007) 970–974.
- [8] D.J. Vanderah, C.W. Meuse, V. Silin, A.L. Plant, *Langmuir* 14 (1998) 6916–6923.
- [9] S.A. Glazier, D.J. Vanderah, A.L. Plant, H. Bayley, G. Valincius, J.J. Kasianowicz, *Langmuir* 16 (2000) 10428–10435.
- [10] R. Valiokas, S. Svedhem, S.C.T. Svensson, B. Liedberg, *Langmuir* 15 (1999) 3390–3394.
- [11] R. Valiokas, M. Ostblom, S. Svedhem, S.C.T. Svensson, B. Liedberg, *J. Phys. Chem. B* 104 (2000) 7565–7569.
- [12] R. Valiokas, S. Svedhem, M. Ostblom, S.C.T. Svensson, B. Liedberg, *J. Phys. Chem. B* 105 (2001) 5459–5469.
- [13] R. Valiokas, M. Ostblom, S. Svedhem, S.C.T. Svensson, B. Liedberg, *J. Phys. Chem. B* 106 (2002) 10401–10409.
- [14] L. Malysheva, Y. Klymenko, A. Onipko, R. Valiokas, B. Liedberg, *Chem. Phys. Lett.* 370 (2003) 451–459.
- [15] L. Malysheva, A. Onipko, R. Valiokas, B. Liedberg, *J. Phys. Chem. A* 109 (2005) 7788–7796.
- [16] L. Malysheva, A. Onipko, R. Valiokas, B. Liedberg, *J. Phys. Chem. B* 109 (2005) 13221–13227.
- [17] L. Malysheva, A. Onipko, R. Valiokas, B. Liedberg, *Appl. Surf. Sci.* 246 (2005) 372–376.
- [18] L. Malysheva, A. Onipko, B. Liedberg, *J. Phys. Chem. A* 112 (2008) 728–736.
- [19] J. Benesch, S. Svedhem, S.C.T. Svensson, R. Valiokas, B. Liedberg, P. Tengvall, *J. Biomater. Sci. Polym. Ed.* 12 (2001) 581–597.
- [20] D.J. Vanderah, R.S. Gates, V. Silin, D.N. Zeiger, J.T. Woodward, C.W. Meuse, G. Valincius, B. Nickel, *Langmuir* 19 (2003) 2612–2620.
- [21] D.J. Vanderah, T. Parr, V. Silin, C.W. Meuse, R.S. Gates, H.Y. La, G. Valincius, *Langmuir* 20 (2004) 1311–1316.
- [22] R. Valiokas, M. Ostblom, F. Björefors, B. Liedberg, J. Shi, P. Konradsson, *Biointerphases* 1 (2006) 22–34.
- [23] M.D. Malinsky, K.L. Kelly, G.C. Schatz, R.P. Van Duyne, *J. Phys. Chem. B* 105 (2001) 2343–2350.
- [24] A. Dmitriev, C. Hagglund, S. Chen, H. Fredriksson, T. Pakizeh, M. Kall, D.S. Sutherland, *Nano Lett.* 8 (2008) 3893–3898.
- [25] J.C. Love, L.A. Estroff, J.K. Kriebel, R.G. Nuzzo, G.M. Whitesides, *Chem. Rev.* 105 (2005) 1103–1169.
- [26] L. Malysheva, A. Onipko, B. Liedberg, *J. Phys. Chem. A* 112 (2008) 1683–1687.
- [27] S. Svedhem, C.A. Hollander, J. Shi, P. Konradsson, B. Liedberg, S.C.T. Svensson, *J. Org. Chem.* 66 (2001) 4494–4503.
- [28] H.-H. Lee, Ž. Ruželė, A. Gutés, F. Björefors, R. Valiokas, B. Liedberg, in preparation.

- [29] U. Gelius, B. Wannberg, P. Baltzer, H. Fellnerfeldegg, G. Carlsson, C.G. Johansson, J. Larsson, P. Munger, G. Vegerfors, J. Electron Spectrosc. Relat. Phenom. 52 (1990) 747–785.
- [30] M. Wirde, U. Gelius, T. Dunbar, D.L. Allara, Modification of Self-Assembled Monolayers of Alkanethiols on Gold by Ionizing Radiation, Elsevier Science Bv, 1997, pp. 245–251.
- [31] G. Beamson, D. Briggs, High Resolution XPS of Organic Polymers: The Scienta ESCA300 database, Wiley, Chichester, 1992.
- [32] L.Y. Li, S.F. Chen, J. Zheng, B.D. Ratner, S.Y. Jiang, J. Phys. Chem. B 109 (2005) 2934–2941.
- [33] S.D. Evans, K.E. Goppertberarducci, E. Urankar, L.J. Gerenser, A. Ulman, Langmuir 7 (1991) 2700–2709.
- [34] T.J. Lenk, V.M. Hallmark, C.L. Hoffmann, J.F. Rabolt, D.G. Castner, C. Erdelen, H. Ringsdorf, Langmuir 10 (1994) 4610–4617.
- [35] R.S. Clegg, S.M. Reed, R.K. Smith, B.L. Barron, J.A. Rear, J.E. Hutchison, Langmuir 15 (1999) 8876–8883.
- [36] D.G. Castner, K. Hinds, D.W. Grainger, Langmuir 12 (1996) 5083–5086.
- [37] H. Rieley, G.K. Kendall, F.W. Zemicael, T.L. Smith, S.H. Yang, Langmuir 14 (1998) 5147–5153.
- [38] L.Y. Li, S.F. Chen, S.Y. Jiang, Langmuir 19 (2003) 2974–2982.
- [39] M.D. Porter, T.B. Bright, D.L. Allara, C.E.D. Chidsey, J. Am. Chem. Soc. 109 (1987) 3559–3568.
- [40] N. Nishi, D. Hobara, M. Yamamoto, T. Kakiuchi, J. Chem. Phys. 118 (2003) 1904–1911.
- [41] F. Tao, S.L. Bernasek, Chem. Rev. 107 (2007) 1408–1453.
- [42] K. Jans, K. Bonroy, R. De Palma, G. Reekmans, H. Jans, W. Laureyn, M. Smet, G. Borghs, G. Maes, Langmuir 24 (2008) 3949–3954.
- [43] S. Xu, S. Miller, P.E. Laibinis, G.Y. Liu, Langmuir 15 (1999) 7244–7251.
- [44] R.G. Snyder, M. Maroncelli, H.L. Strauss, V.M. Hallmark, J. Phys. Chem. 90 (1986) 5623–5630.
- [45] T. Miyazawa, J. Chem. Phys. 35 (1961) 693–713.
- [46] T. Miyazawa, J. Poly. Sci. 55 (1961) 215–231.
- [47] T. Miyazawa, K. Fukushima, Y. Ideguchi, J. Chem. Phys. 37 (1962) 2764–2776.
- [48] A.N. Parikh, D.L. Allara, J. Chem. Phys. 96 (1992) 927–945.
- [49] R.G. Nuzzo, L.H. Dubois, D.L. Allara, J. Am. Chem. Soc. 112 (1990) 558–569.
- [50] L. Bertilsson, B. Liedberg, Langmuir 9 (1993) 141–149.
- [51] O. Dannenberger, K. Weiss, H.J. Himmel, B. Jager, M. Buck, C. Woll, Thin Solid Films 307 (1997) 183–191.
- [52] F. Schreiber, Prog. Surf. Sci. 65 (2000) 151–256.
- [53] R.L.C. Wang, H.J. Kreuzer, M. Grunze, Phys. Chem. Chem. Phys. 2 (2000) 3613–3622.
- [54] R.G. Nuzzo, E.M. Korenic, L.H. Dubois, J. Chem. Phys. 93 (1990) 767–773.